POLITECNICO DI TORINO
Repository ISTITUZIONALE

Model based analysis of precursors of electromechanical servomechanisms failures using an artificial neural network

Original
Model based analysis of precursors of electromechanical servomechanisms failures using an artificial neural network / Battipede, M., DALLA VEDOVA, M.D.L., Maggiore, P., Romeo, S.. - (2015). (AIAA Modeling and Simulation Technologies Conference Kissimmee, Florida 2015) [10.2514/6.2015-2035].

Availability:
This version is available at: 11583/2588180 since: 2020-12-14T18:47:00Z

Publisher:
AIAA

Published
DOI:10.2514/6.2015-2035

Terms of use:

This article is made available under terms and conditions as specified in the corresponding bibliographic description in the repository

Publisher copyright

(Article begins on next page)

30 June 2026

Model based analysis of precursors of electromechanical servomechanisms failures using an artificial neural network

Manuela Battipede[1], Matteo D. L. Dalla Vedova[2], Paolo Maggiore[3] and Simone Romeo[4]
Politecnico di Torino, Turin, Italy, 10129

Several approaches can be employed in prognostics, to detect incipient failures of primary flight command electromechanical actuators (EMA), caused by progressive wear. The development of a prognostic algorithm capable of identifying the precursors of an electromechanical actuator failure is beneficial for the anticipation of the incoming failure: a correct interpretation of the failure degradation pattern, in fact, can trig an early alert of the maintenance crew, who can properly schedule the servomechanism replacement. Prognostic, though, is strictly technology-oriented as it is based on accurate analysis of the cause and effect relationships. As a consequence, it is possible that prognostics algorithms that demonstrate great efficacy for certain applications (electrohydraulic actuators, for examples) fail in other circumstances, just because the actuator is based on a different technology. The research presented in this paper proposes a prognostic technique able to identify symptoms of an EMA degradation before the actual exhibition of the anomalous behavior; to this purpose friction, backlash, coil short circuit and rotor static eccentricity failures are considered. An innovative model-based fault detection neural technique is proposed to analyze information gathered through FFT analysis of the components under normal stress conditions. A proper simulation test bench was developed: results show that the method exhibit adequate robustness and a high degree of confidence in the ability to early identify an eventual malfunctioning, minimizing the risk of false alarms or unannunciated failures.

ANN	=	Artificial Neural Network
ΔV_{ij}	=	ij-th phases differential voltage
$\dot{\theta}_{rM}$	=	effective rotor speed
e_{ij}	=	ij-th phases back-EMF
EMA	=	electromechanical actuator
FFT	=	Fast Fourier Transform
ke_i	=	i-th back-EMF constants
K_{tr}	=	EMA transmission shaft stiffness
I_i	=	actual i-th phase currents
I_{ref}	=	reference current
I_{ref_i}	=	reference i-th phase current
V_i	=	effective i-th phase voltages
V_{ij}	=	ij-th phases line-to-line voltage
θ_{rM} , θ_{rU}	=	EMA motor or user position
TM	=	BLDC motor torque
TR	=	external aerodynamic torques
T_{reaz}	=	EMA transmission shaft reaction torque

[1] Associate Professor, Department of Mechanics and Aerospace Engineering, Corso Duca degli Abruzzi 24, manuela.battipede@polito.it
[2] Research Assistant, Department of Mechanics and Aerospace Engineering, Corso Duca degli Abruzzi 24, matteo.dallavedova@polito.it.
[3] Associate Professor, Department of Mechanics and Aerospace Engineering, Corso Duca degli Abruzzi 24, paolo.maggiore@polito.it.
[4] MSc student, Department of Mechanics and Aerospace Engineering, Corso Duca degli Abruzzi 24, simone.romeo@studenti.polito.it.

I. Introduction

PROGNOSTICS purpose is to predict when a certain component loses its functionality and is not further able to be fully operative or to meet the desired performances. Such a discipline is based on the analysis and comprehension of all the possible failure modes and on the capability of individuating the first symptoms of aging or wear. Once properly gathered and organized, such a database can be effectively used as an input of a proper failure propagation model. As for the other technological domains, applying prognostics to aeronautics could have a beneficial impact on the maintenance aspect, as it could reduce both costs and inspection time. The goal of this discipline, named Prognostics and Health Management (PHM), is to provide real-time data of the current status of the system and to calculate the Remaining Useful Life (RUL) before a fault occurs with the consequence that a component becomes unable to perform its functionalities at the desired level. The advantage of implementing PHM clearly emerges from the comparison with classical monitoring and maintenance concepts, based on overhaul or life-limited parts. The primary flight controls, for example, are a critical part of the aircraft system and are therefore designed with a conservative safe-life approach, which imposes to replace the related components after having endured a fixed amount of flight hours or operating cycles. Obviously, when applying this approach, the effective status of the components is not assessed and maintenance is limited to the specific scheduled operation. In particular, the safe-life design criterion lacks of the possibility of evaluating initial flaws, which might derive from the manufacturing process and could degenerate in a sudden fault that compromises the aircraft safety. In fact, the progressive degradation of a system component, which initially does not create an unacceptable behavior, often leads to a condition in which the efficiency of such component is impaired, with the consequence that the actuator functionality is compromised. The safe-life criterion, moreover, does not allow the individuation of the malfunctioning cause and location, whereas an accurate identification of which specific subcomponent has failed could be effective in reducing maintenance inefficiencies and costs, as the replacement of the single subcomponent, instead of the whole system, could be sufficient to restore the system functionality. By applying PHM strategies, failures could be managed in a more effective way, with the following benefits:

1) operating costs are diminished;
2) less maintenance interventions are required;
3) the amount of necessary redundancies is reduced;
4) aircraft safety and reliability are improved;
5) logistic is simplified, as maintenance actions can be planned appropriately with the immediate outcome that downtime and related costs are limited and the management of spare parts warehouses is more effective.

It must be noticed that the prognostic concepts, because of the variety of applications and the huge impact that they generate, have aroused great interest in the scientific and technological world and, especially in recent years, have been the subject of extensive development and dissemination in the scientific literature. Very often these contributions, despite being extremely innovative and significant, result too theoretical or specific and tend to overlook a more comprehensive approach (i.e. systemistic vision), dwelling on well-defined and circumscribed aspects of the considered problem.

In this paper the authors propose a more systemistic and multidisciplinary approach, in which the different aspects of the considered problem, concerning the electrical and mechanical characteristics of the actuator and its relevant failure modes, have been analyzed and modelled together in the same multi-domain numerical model. In particular, the research presented in the paper is focused on a fault detection/evaluation technique able to identify the failure precursors and evaluate the corresponding damage entity. To this purpose, a relatively accurate numerical model of the actuation system and its failure modes have been implemented, in the MATLAB Simulink® simulation environment, to analyze the EMA performance and the effects of different progressive faults. Several sets of simulations have been performed, encompassing nominal conditions and various failure modes. The numerical analysis of the Fast Fourier Transform of the closed loop signals have been used to single out the proper precursors of specific faults that can be effectively detected/evaluated by an innovative neural prognostic algorithm.

To assess the actual ability of the algorithms to correctly sort out the failure precursors, an appropriate simulation test bench has been developed, based on the injection of an irregular degradation pattern into the flight control system. Results show that the method exhibits adequate robustness and a high degree of confidence in the ability to early identify an eventual malfunctioning, minimizing the risk of false alarms or unannunciated failures.

To ensure the feasibility of the application on the proposed prognostic method on aircraft in the civil aviation category, real-time inflight analysis is not implemented: this technique specifically refers only to preflight/postflight or ordinary maintenance procedures, when the data can be analyzed by an external computer without affecting the normal inflight operations. These algorithms can be easily integrated in an automatic system check process, which can be performed by the maintenance staff.

The built-in test can be executed without the component disassembly and requires a simple postprocessing and analysis of the downloaded data. Moreover, in order to avoid the introduction of new sensors or additional components, the proposed algorithms use only information gathered from transducers that already equip the considered system or that are derived from virtual sensors which post-process the actual raw measurements.

II. Primary Flight Control EMAs

Primary flight controls are typically proportional servomechanisms with continuous activation: they must return a force feedback related to command intensity and a high frequency response. Since their loss is a critical issue, their reliability must be very high. Their purpose is to control the dynamic of the aircraft by generating, by means of the rotation of the corresponding aerodynamic surfaces, unbalanced forces/couples acting on the aircraft itself. These controls are usually conceived to obtain the aircraft rotation around one of the three body axis when one control surface is activated, possibly minimizing the coupling effects. Depending on the actuation mode of the primary control surfaces, a flight control system can be classified as reversible or irreversible. The first type of system provides a direct mechanical linkage connection between the flight control surface and the control lever. The pilot must compensate the hinge moment generating an adequate force: hinge moment is mainly related to primary surface sizes, to their deflection in airstream, to aircraft speed and it could be lowered by using proper aerodynamic compensation. Vice versa, irreversible flight control systems do not require a pilot's action to compensate the hinge moment and utilize command lines that can be mechanical, electrical (fly-by-wire) or optical (fly-by-light). Until a few years ago, the actuators mainly used in aeronautical applications were generally hydraulic and precisely hydromechanical or, more recently, electrohydraulic. This kind of actuator, because of its great accuracy, high specific power and very high reliability, is often equipped on current aircrafts, even if on more modern airliners electro-hydrostatic actuators (EHA) or electro-mechanical actuators (EMA) are installed. In EHA, highly-pressurized hydraulic fluid is maintained only near the actuator, whereas otherwise the hydraulic line is replaced by an electric signal, which allows a consistent weight reduction. In this case, the actuator usually consists of an electrical motor that converts electrical power into mechanical power, which is then transformed into hydraulic power by means of an axial piston pump. Finally, a linear or a rotary actuator can be employed, depending on the architecture. Even if the EHAs provides attractive benefits and represents an interesting alternative to traditional hydraulic controls, in the last years the trend towards the all-electric aircrafts brought to an extensive application of novel optimized electrical actuators, such as the electromechanical ones (EMA). To justify the fervent scientific activity in this field and the great interest shown by the aeronautical world, it must be noticed that, compared to the electrohydraulic actuations, the EMAs offer many advantages: overall weight is reduced, maintenance is simplified and hydraulic fluids, which is often contaminant, flammable or polluting, can be elimination. For these reasons, the use of actuation systems based on EMAs is increasing in various fields of aerospace technology. In the framework of the COVADIS project, an EMA has been developed and produced by Sagem and flew for the first time in January 2011, as the primary flight control for the aileron on an Airbus A320 commercial jet. EMAs have also become attractive candidates to replace hydraulic actuators for Thrust Vector Control (TVC) of launchers, thanks to an easier implementation and lower maintenance requirements. The TVC is a subsystem which controls the direction of gimballed nozzles of rocket engines, following the request/command from the launcher trajectory and attitude control system. In that case EMAs are currently under ESA development for the VEGA launcher and studied in the framework of the Future Launchers Preparatory Programme for Next Generation Launchers (NGL).

Finally, Air Force Research Laboratory, AFRL/RQQM Mechanical & Thermal Systems Branch, has launched a program to develop a robust, thin-wing primary flight actuator, capable of achieving a high-duty cycle application (e.g. aileron) while fitting within the volume constraints, which is mandatory in future thin-wing aircraft design.

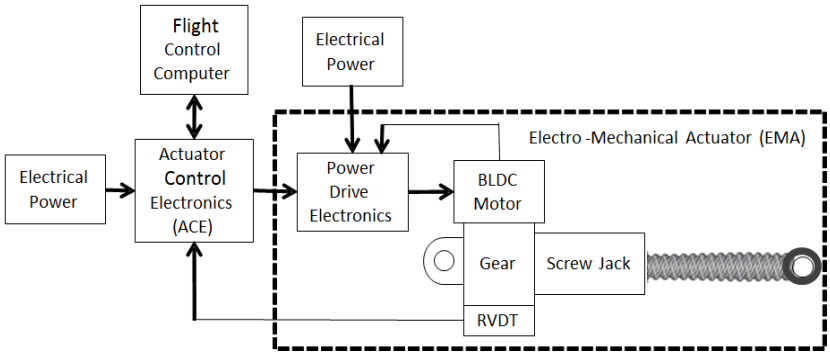

Figure 1. EMA scheme.

As shown in Fig.1, a typical electromechanical actuator used in a primary flight control is composed by:

1) an actuator control electronics (ACE) that closes the feedback loop, by comparing the commanded position (FBW) with the actual one, elaborates the corrective actions and generates the reference current I_{ref};
2) a Power Drive Electronics (PDE) that regulates the three-phase electrical power;
3) an electrical motor, often BLDC type;
4) a gear reducer having the function to decrease the motor angular speed (RPM) and increase its torque to desired values*;
5) a system that transforms rotary motion into linear motion: ball screws or roller screws are usually preferred to acme screws because, having a higher efficiency, they can perform the conversion with lower friction;
6) a network of sensors used to close the feedback rings (current, angular speed and position) that control the whole actuation system (reported in Fig. 1, as RVDT).

III. Proposed Actuation System Numerical Model

As previously mentioned, the primary goal of this research is to propose a technique to identify precocious symptoms of an EMA degradation. In order to assess feasibility performance and robustness of the aforesaid technique, a suitable simulation test environment has been developed in the MATLAB/Simulink® environment. The proposed scheme, reported in Fig.2, is consistent with the EMA architecture shown in Fig.1.

As shown in Fig. 2, the EMA is composed by six different subsystems:

1) an input block that generates the different position commands (block Com);
2) a subsystem simulating the actuator control electronics, that closes the feedback loops and generates in output the reference current I_{ref} (block ACE);
3) a subsystem simulating the power drive electronics and the trapezoidal BLDC electromagnetic model, that evaluates the torque developed by the electrical motor as a function of the voltages generated by the three-phase electrical power regulator (block BLDC EM Model);
4) a subsystem simulating the EMA mechanical behavior by means of a 2 degree-of-freedom dynamic system (block EMA Dynamic Model);
5) another input block simulating the aerodynamic torques acting on the moving surface controlled by the actuator (block TR);
6) a block simulating the monitoring system (block Monitor).

The numerical model includes the effects of the analogic to digital conversion of the feedback signals, the electrical noise acting on the signal lines and the electrical offset of the position transducers.

Fig.3 shows the brushless DC motor electromagnetic model (block BLDC EM Model): it is composed by three blocks representing the reference current generator, the three-phase PWM inverter system and the BLDC motor electromagnetic model.[1,2]

The trapezoidal back-EMF and the electrical current waveforms of the three-phase BLDC motor, evolving as a function of the rotor position θ_{rM}, are shown in Fig.4.

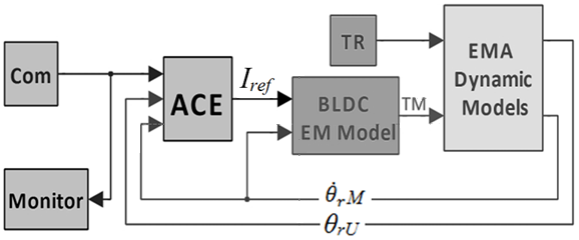

Figure 2. Proposed EMA block diagram.

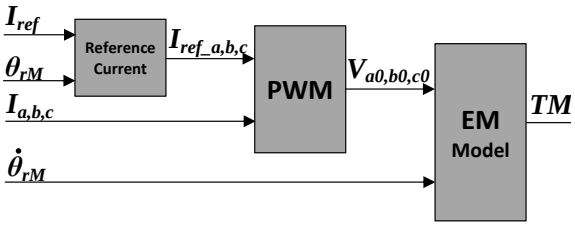

Figure 3. BLDC EM Model block diagram.

Table 1. Reference Currents of BLDC Motor

Rotor Position [Deg]	Reference Currents [Amp]		
	I_{ref_a}	I_{ref_b}	I_{ref_c}
0-30	0	$-I_{max}$	I_{max}
30-90	I_{max}	$-I_{max}$	0
90-150	I_{max}	0_x	$-I_{max}$
150-210	0	I_{max}	$-I_{max}$
210-270	$-I_{max}$	I_{max}	0
270-330	$-I_{max}$	0	I_{max}
330-360	0	$-I_{max}$	I_{max}

* The RPM or torque variations are obviously related to the gear ratio of the mechanical reducer. The output torque (after the reducer) is also affected by the efficiency of the mechanical transmission.

As shown in Table I, the Reference Current generator determines the motor reference phase currents, I_{ref_a}, I_{ref_b}, and I_{ref_c}, by considering the reference current amplitude I_{ref}, which is calculated depending on the rotor position.[1] The PWM current control block simulates the inverter behaviour comparing the reference phase currents I_{ref_a}, I_{ref_b} and I_{ref_c} with the motor actual phase currents I_a, I_b and I_c. As a matter of fact, the considered block diagram does not implement the structure and the real operation of the three-phase PWM inverter: its behavior is simulated by means of a relay block, with proper thresholds that can be set for each phase. The output of this subsystem is a rotating voltage vector having three *120°* degrees displacement components, one for each phase, representing the corresponding phase voltages V_{a0}, V_{b0} and V_{c0}.

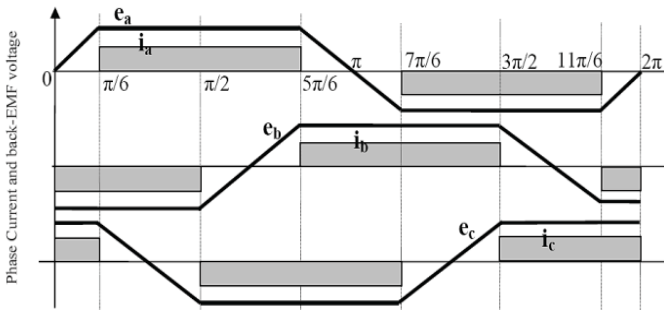

Figure 4. Phase back-EMF and current waveforms of a three-phase BLDC motor.

As for the I_{ref} calculation, at a same instant the first phase has a positive value, the second phase has a same absolute value with negative sign, the third phase must be null (even if not identically null, at least the mean value must satisfy this property).

The EM Model block calculates the three-phase currents, I_a, I_b and I_c, and the developed mechanical torque *TM* as a function of the PWM three phase voltages (V_{a0}, V_{b0}, V_{c0}) and the effective rotor speed $\dot{\theta}_{rM}$.

The considered BLDC motor has a three-phase winding topology with star connection: it has three resistive (*R*) – inductive (*L*) branches on which a counter-electromotive force (back-EMF) acts. The back-EMF phase voltages are implemented in look-up table form.[2] In nominal conditions and no failure the back-EMF, acting on each phase, is a function of the rotor position θ_{rM} and the amplitude is defined by $e_a = ke \cdot \dot{\theta}_{rM}$, where *ke* is the back-EMF constant of the considered phase. In case of an electrical failure, such as coil short-circuits or static eccentricity, the back-EMF constants ke_i (one for each of the three branches) can be adjusted to represent the failure effect by means of three functions *f(u)*, one for each motor phase. To calculate the value of the three phase currents, I_a, I_b and I_c, it is necessary to evaluate the differential voltage acting on each phase. As shown in Fig. 5, the proposed model considers the three-phase currents in terms of the line-to-line voltages (i.e. the differential voltage between two of the three phases). These differential voltages, ΔV_{ab}, ΔV_{ac}, and ΔV_{bc}, are calculated as the difference between the corresponding line-to-line values of voltage, V_{ab}, V_{ac}, and V_{bc}, and back-EMF, e_{ab}, e_{ac} and e_{bc}:

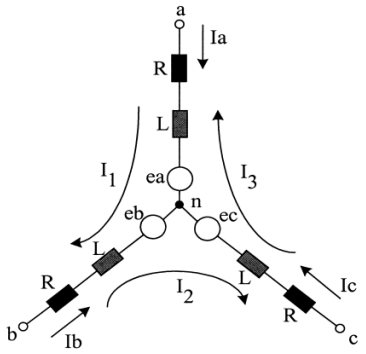

Figure 5. Schematic of voltage and current parameters in three-phase BLDC motor.

$$\begin{aligned} \Delta V_{ab} &= V_{ab} - \mathrm{e}_{ab} = R_{LL} I_1 + L_{LL} \frac{dI_1}{dt} \\ \Delta V_{bc} &= V_{bc} - \mathrm{e}_{bc} = R_{LL} I_2 + L_{LL} \frac{dI_2}{dt} \\ \Delta V_{ca} &= V_{ca} - \mathrm{e}_{ca} = R_{LL} I_3 + L_{LL} \frac{dI_3}{dt} \end{aligned} \tag{1}$$

Once the line-to-line differential voltages have been calculated, it is possible to derive the three phase currents, I_a, I_b and I_c, according to Eq. (2):

$$\begin{aligned} I_a &= I_1 - I_3 \\ I_b &= I_2 - I_1 \\ I_c &= I_3 - I_2 \end{aligned} \tag{2}$$

Once the phase currents are known, total motor torque can be estimated as the sum of the three phase currents, multiplied by their respective back-EMF constants *ke*. The obtained mechanical motor torque *TM*, then, must be limited by a saturation function as in real actuator every component is subject to operative limitations. To validate the model, the dynamic response developed by the system under specific operating conditions, in terms of control input, boundary conditions and entities of different faults, was compared with data obtained from the current literature. In particular a fairly good match with literature data has been noticed on the back-EMF and phase current waveforms, related to different values of the rotor angular velocity and the dynamic responses of the BLDC, caused by various command input.[3-5] The subsystem EMA Dynamic Model of Fig.2 simulates the EMA mechanical behavior. As shown in Fig.6, it consists of two non-linear second order dynamic models, which simulate, respectively, the BLDC motor/gear reducer (BLDC Motor) and the aircraft command surface controlled by the EMA (USER); they are linked together by means of an elastic shaft. The model includes effects of the dry friction forces developed in rotor bearings, gear reducer, hinges and screw actuators.[6]

In particular, the frictional torque is accounted for as proposed in Ref. 7 and Ref. 8. The subsystem Mechanical Transmission models the behavior of the transmission shaft that connects the gear-motor assembly to the aircraft command surface. The corresponding reaction torque T_{reaz} is calculate as a function of θ_{rM} and θ_{rU} (respectively the motor and user position) and K_{tr}, which represents the stiffness of the transmission shaft. The effects of the mechanical backlashes are also considered.[9]

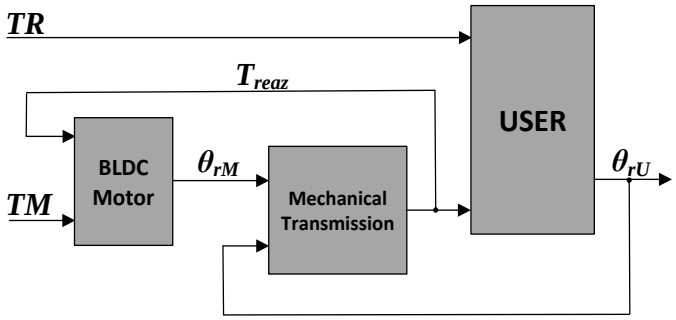

Figure 6. EMA Dynamic Models block diagram.

IV. EMA Failures and Degradations

As EMA have been only recently employed in aeronautics, their cumulated flight hours are still not enough to provide reliable statistics data about more recurring failures. However, it is possible to single out four main failure categories: mechanical or structural failures, BLDC motor failures, electronics failures and sensor failures.

The present work has been mainly focused on the effects of mechanical failures due to progressive wear, which causes an increase of backlash and friction, and on two typical BLDC motor failures: the coil short-circuits (SC) and the bearing wear generating rotor static eccentricity (RE). As a general rule, the detection/evaluation of mechanical failure due to friction or backlash is usually directly performed by analyzing specific characteristics of the dynamic response of the whole actuation system, such as position, speed or acceleration. Vice versa, in case of motor progressive failures, such as SC or RE, the characteristics of the mechanical transmission, in terms of inertia, dry and viscous frictions, backlashes, noises, etc., could disguise or mitigate the failure effects making inaccurate, if not ineffective, any prognostic effort. In these cases the analysis of electrical harmonics (e.g. phase currents) provides a better understanding of the failure progression and its estimation is far more accurate. Electrical and sensor failures are not less important than the others, but their evolutions are usually very fast, if not instantaneous, and the corresponding failure precursors are often difficult to identify and evaluate. It is well known that the dry friction phenomena always occur when two surfaces are in relative motion: when the friction coefficient increase due to wear, the reaction torque increases accordingly and the motor must provide higher torques to actuate the control surface. As a primary effect, an increment in dry friction, well before causing the seizure of the entire system, reduces the servomechanism accuracy and, sometimes, influences the system dynamic response generating unexpected behavior, such as stick-slip or limit cycles.[10]

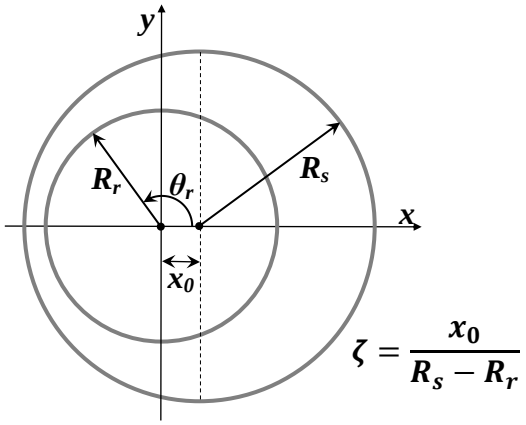

Figure 7. Reference system for the definition of air gap.

The mechanical wear can also generate backlash in EMA moving parts such as gears, hinges, bearings and especially screw actuators. These backlashes, acting on the elements of the mechanical transmission, reduce the EMA accuracy and can lead to problems of stiffness and controllability of the whole actuator.[11]

BLDC motor failures are mainly seen as progressive coil short-circuits or bearing wear generating rotor static eccentricity. Short-circuits usually start between a few coils belonging to the same phase (coil-coil failure). As in short-circuited coils the voltage remains the same and the resistance decreases, the resulting currents increases, generating a localized temperature rising in conductor, which favors the extension of the failure to adjacent coils. If this kind of failure is not promptly detected it could propagate and generate phase-phase or phase-neutral damages.

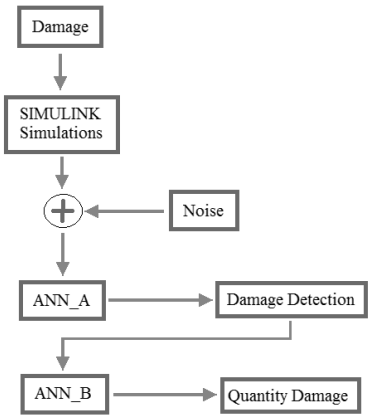

Figure 8. ANN model

The static eccentricity of a rotating body consists in a misalignment between the rotor rotation axis and the stator axis of symmetry. This misalignment is mainly due to tolerances and imperfections introduced during motor construction or to a gradual increase of wear of the rotor shaft bearings. When this failure occurs, the motor having more than one polar couple generates a periodically variable magnetic flux, as the air gap varies during its 360° degrees turn. In case of static eccentricity, the air gap changes during the rotor spinning (Fig.7) as a function of the rotor position θ_r:

$$g'(\theta_r) = g_0 + x_0\cos(\theta_r) \tag{3}$$

where g_0, is the clearance between stator and rotor, without considering misalignments, and the second term represents the variation of the air gap. In terms of motor performances, the provided torque is lower than in nominal conditions, whereas, spectral analysis reveals the presence of sub-harmonics which increase for higher eccentricities. The rotor static eccentricity and the partial stator coil short circuit effects have been modeled by means of a simplified numerical algorithm. As both the failures change the magnetic coupling between stator and rotor, in fact, failures can be modelled by modifying the values and angular modulations of the back-EMF coefficients[†]:

$$ke_a = ke_a \cdot Ce_a \cdot (1 + \zeta\cos(\theta_r)) \tag{4}$$

where ζ is the rotor static eccentricity. The constants ke_a, ke_b and ke_c are then used to calculate the corresponding counter-electromotive forces, e_a, e_b and e_c, and to evaluate the mechanical couples, Ce_a, Ce_b and Ce_c, generated by the three motor phases. The effects that the abovementioned progressive failures produce on the dynamic behaviors of the considered actuation system are thoroughly discussed in Ref. 12.

V. Proposed Prognostic Algorithm

As previously reported, an innovative model based fault detection technique, based on neural identification, is proposed as a prognostic method which analyzes data obtained through FFT spectral analisys.[13,14]

In particular, this method is based on two distinct Multi-Layer Perceptron (MLP) Neural Networks (NN), each one designed and trained to perform a specific task[15]: the first neural network (ANN_A) detect the damage and classify it according to a predefined classification scheme, whereas the second network (ANN_B) provides a measure of the fault extent, according to a quantification scheme.

A. Data Collection / Preprocessing

The command input used for the data collection is a step signal *Com* and the data are recorded immediately after the transient. Values of speed and currents are recorded in two matrices: they refer to situations of a growing level of the fault gravity, where the failure extent can vary within a range considered sustainable and realistic for the engine. Increments of the failure extents are discrete: they are moderate but noticeable, to highlight the differences between two successive cases. Furthermore, random noise is added to the simulation signals to improve the network

[†] The proposed algorithm, implemented in the BLDC EM Model block diagram, acts on the three back-EMF constants Ce_i (one for each branch) modulating their trapezoidal reference values Ke_i as a function of coil short circuit percentage, static rotor eccentricity ζ and angular position ϑ_r.

robustness. To test the noise amount that can be tolerated by the prognostic algorithm, signals are corrupted with three different noise levels, including the noise free situation (0%), the high noise case (5% of the maximum signal value) and an intermediate situation for which the noise level is halved (2.5%). The data processed by the two neural networks (ANN_A and ANN_B) are mainly based on macro-observations of the behavior of the speed and currents and on the spectral analysis of signals.

B. Phase Current analysis

In this subsection the signal features, derived as a consequence of a fault condition, are identified and mathematically defined. Trends related to the growing failure extent are also discussed. The main difference between Fig. 9 and Fig. 10, which reports two different failures, concerns the distribution of the concavity of the phase current signals, in correspondence of the two-PhaseON (TPO) phenomena. By approximating this part of the signal with a second degree equation and by varying the extent of the fault, it is observed that the failure to static rotor eccentricity (RE) presents, for each phase, concavity that are always positive. Conversely, the short-circuit (SC) fault presents an alternation of the signs of the concavity: two negatives and one positive in the TPO positive portion and vice versa, two positives and one negative when the TPO is the negative. Another observation concerns the signal symmetry: analyzing all the positive and negative TPO sections as a single signal, a sort of envelope, it can be noticed that, in case of SC, the positive and negative signals are symmetrical with respect to the horizontal axis, whereas in the case of RE, these signals are simply shifted. It must be noticed that the evaluation of the maximum and average trends of these current signals plays an important role in the failure detection: as the fault extent increases, in fact, the maximum value increases monotonously for the SC fault, whereas the RE failure exhibit a constant trend followed by a rapid growth. The average value has a monotonous increasing behavior in the SC fault whereas for the RE, the trend shows an oscillating behavior around a mean value.

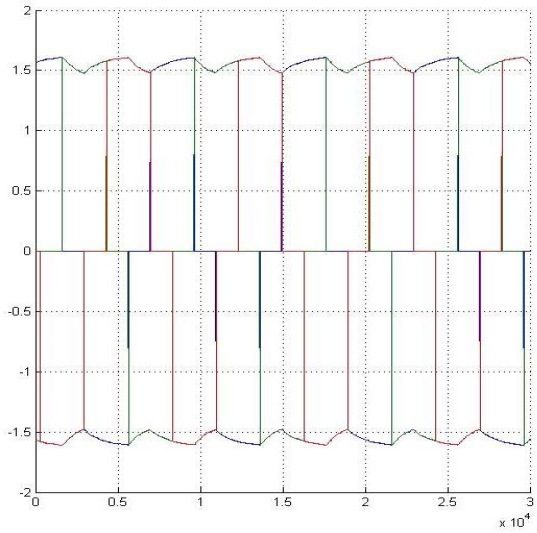

Figure 9. Reference current signal, 25% short-circuit fault entity

C. Speed analysis

As for the speed signals, the main differences for the two faults can be observed through the FFT analysis. As shown in Fig.11, in fact, the SC fault features clear signature marks for four characteristic frequencies around the values of 0 Hz, 251 Hz, 503 Hz and 755 Hz. In particular, the gains associated with these frequency values are characterized by a trend which changes monotonously with the increase of the fault extent. The RE fault exhibits a similar behavior, but the three characteristic frequencies are around the values of 0 Hz, 122 Hz, and 375 Hz (Fig.12)

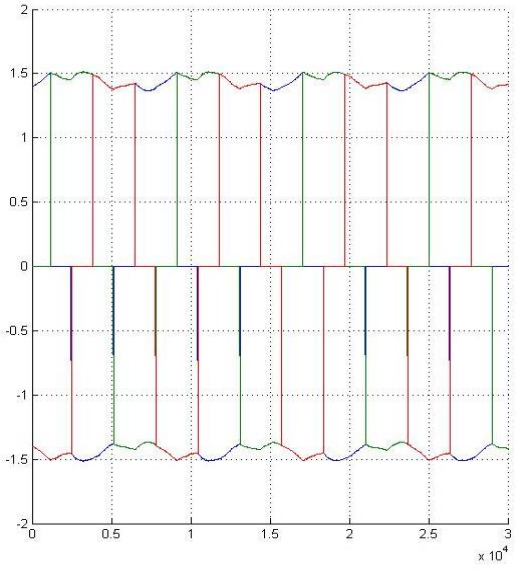

Figure 10. Reference current signal, 5% rotor eccentricity fault entity

D. ANN_A

The first neural network (ANN_A) has the task to perform the first fault detection and classification, through a two class separation: SC fault on the stator coils and RE fault. The network is trained to associate the training vector *P* to the target vector *T*.

The training set *P* consists of 3 sections, each one characterized by a different noise level, organized on 42 rows each. Each row contains 7 elements: the first three elements indicate, by means of the values +1 or -1, the three positive PhaseON concavities, the fourth and the fifth ones indicate the frequency of the two main carrier frequencies; the sixth and seventh show, respectively, the maximum value and the mean value of the envelope signal of the three PhaseON.

The vector target *T* consists of three equal sections of 42 rows each for 2 columns. Each row of the vector *T* is associated with a row of the vector *P*. The first column represents the SC fault, whereas the second column represents the RE failure. The training set is manually generated from a properly dimensioned matrix of zero elements, where unitary values are inserted in the appropriate column, to give the neural network the indication related to which fault type the corresponding row of the training vector belongs. In this context, the ANN_A essentially perform a pattern recognition task and is morphologically shaped as a single-hidden-layer perceptron, with a Log-Sigmoid activation function on the hidden layer.

Training is performed by the Levenberg-Marquardt backpropagation algorithm.[16,17]

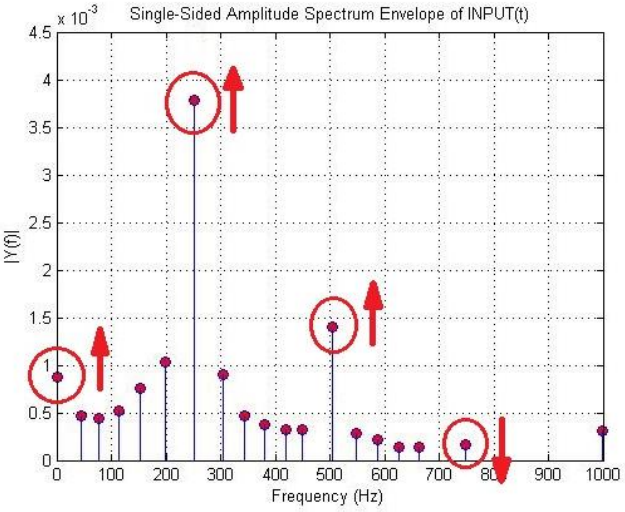

Figure 11. Short circuit failure: example of related EMA angular speed FFT

E. ANN_B

The second neural network (ANN_B) provides a quantification of the failure extent. To assess two different failures, ANN-B is doubled in two parallel neural networks, each specialized for a single type of fault. After the first network ANN_A perform its first classification task, only one branch of ANN_B is activated according to which of the two failures has been detected. The two ANN_B have the same macro-structure of the ANN_A, with 3 sections, each one characterized by a different noise level, composed by a certain number of row and elements.

The SC training vector consists of 21 row, each one containing 11 elements: the first four elements indicate the amplitudes of the four characteristic peaks of the FFT speed signal (frequency: 0 Hz, 251 Hz, 503 Hz and 755 Hz); the fifth and the sixth element show, respectively, the maximum value and the mean value of the envelope signal of the three PhaseON. The last five elements represent the first five peaks of the current FFT. The SC target vector consists of 3 equal sections of 21 rows each. Assuming a classification pattern constituted by three levels of failure (small / medium / large), the target vector is composed of three columns: the first column represents failures of small entities, the second one is related to failures of medium entities and the third column refers to failures of great magnitude. Also in this case, this vector is initially identically null, but inserting a unitary value into the appropriate column, it is possible to indicate to the neural network in which fault category the corresponding row of the training vector belongs.

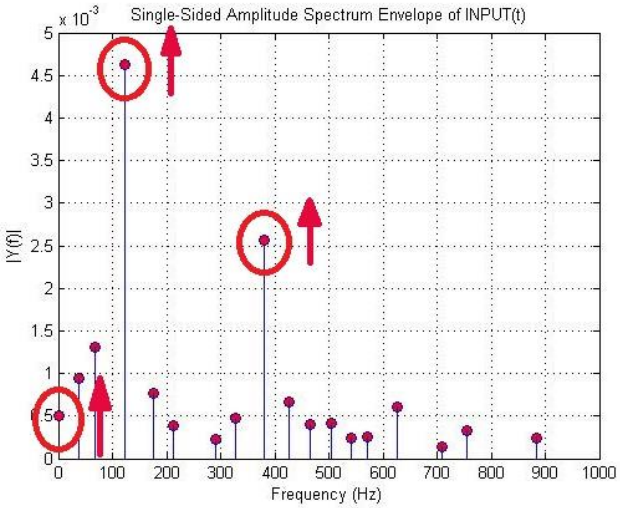

Figure 12. Rotor eccentricity: example of related EMA angular speed FFT

It is also possible to divide the failure range in more than three levels, provided the training set contains a fair amount of information related to each fault level. The RE training vector consists of 21 row, each one containing 12 elements: the first three elements indicate the amplitudes of the three characteristic peaks of the FFT speed signal (frequency: 0 Hz, 122 Hz and 375 Hz); the fourth and the fifth element show, respectively, the maximum value and the mean value of the envelope signal the three PhaseON; the sixth and seventh element represent the relationship

between the maximum value and the minimum value of the speed signal, and between the maximum value and the mean value of the speed signal; the last five elements represent the first five peaks of the current FFT.

As for the ANN_A, also the two ANN_B neural networks perform a pattern recognition task. They have identical morphologies, but different dimensions, determined as a result of an optimization procedure.

VI. Results

The three networks provide results in form of row vectors: each element represents the percentage of probability that the input corresponds to the fault indicated by the target vector column. Ideally, the ANN_A network should always respond with an output in the form $Y = \mathrm{sim}(\mathrm{net}, P_{\mathrm{tester}}) = [1 \quad 0]$ to an input of SC, whereas, in case of RE, it should respond with vector $[0 \quad 1]$. As shown in Table 2 and 3, the obtained results are very close to the theoretical values.

Table 2. SC fault recognition

hort-circuit fault	Y = sim (net, P_{tester})	
Fault entity	-	-
97%	0.9999	0.0001
91%	1	0
80%	1	0
70%	1	0

Table 3. RE fault recognition

Rotor eccentricity fault	Y = sim (net, P_{teste}	
Fault entity	-	-
0,4%	0.0009	0.999
0,9%	0.0009	0.9991
1,8%	0.0009	0.999
3.2%	0.0009	0.9988

The two ANN_B networks, used for the quantification of the SC and RE failure, are based on particular target vectors: the target vectors are structured with an element which is shared between the two entities representing two different fault level. This element is called *intersection* and is effective in widening the fault detection capability. It is observed that around the intersections there are bands of interference, i.e. range of fault percentages (from 2% up to 5%) in which both fault level are perceived. Results are shown in table form, both for the two and three levels classification.

Short-circuit fault 2 columns target vector	Y = sim (net, P_{tester})	
Fault entity	Small	Large
96%	1	0
89%	1	0,0002
87%	1	0
85%	0,997	0,997
84%	0,6136	1
83%	0,7543	0,991
82%	0,0442	1
80%	0,0038	0,9998
76%	0,0002	0,9999

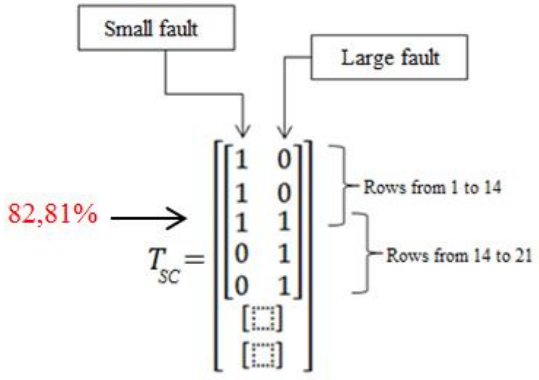

Figure 13. SC fault analysis - two columns target vector

Short-circuit fault 3 columns target vector	Y = sim (net, P_{tester})		
Fault (% of coil turns)	Small	Medium	Large
4%	0,9868	0,0805	0,0015
6%	0,8771	0,3062	0,001
8%	0,785	0,8001	0,009
9%	0,5942	0,8042	0,0005
10%	0,0873	0,9904	0,0008
11%	0,0012	0,9993	0,0004
15%	0,0011	0,9967	0,0015
17%	0,0001	0,4689	0,2992
18%	0,0001	0,9325	0,0854
19%	0	0,0597	0,9543
20%	0	0,0778	0,9861
21%	0	0,0612	0,998
24%	0	0,0151	0,9997

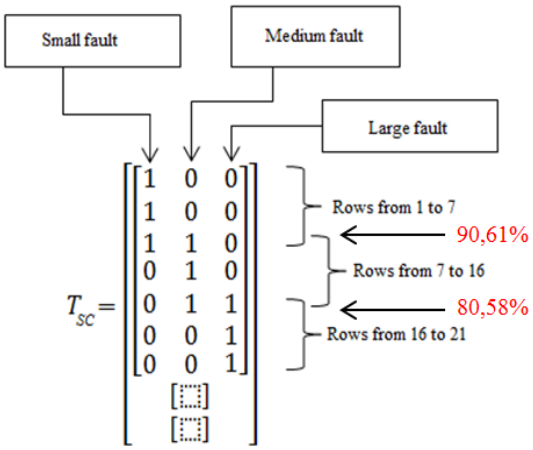

Figure 14. SC fault analysis - three columns target vector

From the technical point of view, nothing prevents to increase the fault levels to more than three. The analysis performed on more than four fault levels, though, show that the interference band widen to such an extent that the network detection capability is impaired. This result represents only a theoretical limitation, however, as widening the level classification beyond a certain level would bring no real benefit to the prognostic analysis, with the only outcome of possible misinterpretation of result.

Rotor eccentricity fault 2 columns target vector	Y = sim (net, P_{tester})	
Fault entity	Small	Large
0,48%	0,9464	0,1076
0,80%	0,6164	0,2083
1,30%	0,6092	0,5441
1,80%	0,0969	0,7088
2,00%	0,047	0,8786
2,20%	0,6746	0,6258
2,80%	0,0576	0,9884

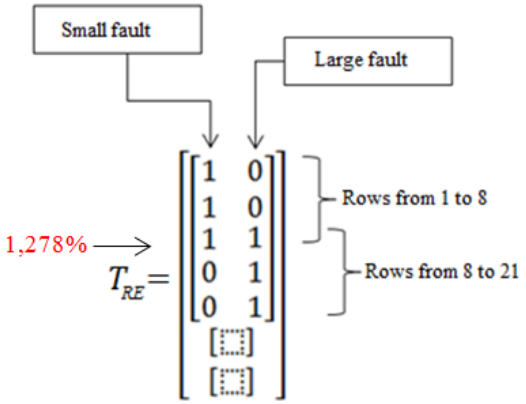

Figure 15. RE fault analysis - two columns target vector

VII. Conclusions

Although the employed neural networks are very simple and have not been optimized, preliminary results shows that the proposed prognostic technique is effective for the diagnosis of the state of a BLDC motor. Only two faults have been analyzed for this paper, short-circuit of a stator coil and static eccentricity of the rotor, and no attempt has been made to consider the cross effects. Results encourage the extension of the technique to investigate more challenging occurrences, such as the electrical and sensor failures, for which the evolutions are usually very fast, if not instantaneous, and the corresponding failure precursors are often difficult to identify and evaluate. To this purpose the actuator model should be further detailed and new element should be modelled. Combined failures should also be investigated.

Short-circuit fault columns target vector	Y = sim (net, P_{tester})		
Fault entity	Small	Medium	Large
0,48%	0,3929	0,1382	0,0211
0,80%	0,0472	0,962	0,0021
1,00%	0,0488	0,8019	0,0563
1,20%	0,0002	0,9939	0,2283
1,30%	0	0,9973	0,5215
1,40%	0	0,9975	0,7143
1,80%	0,0002	0,9956	0,3476
2,00%	0	0,9908	0,8168
2,20%	0,0002	0,9996	0,4527
2,30%	0	0,2894	0,983
2,80%	0	0,0048	0,9997

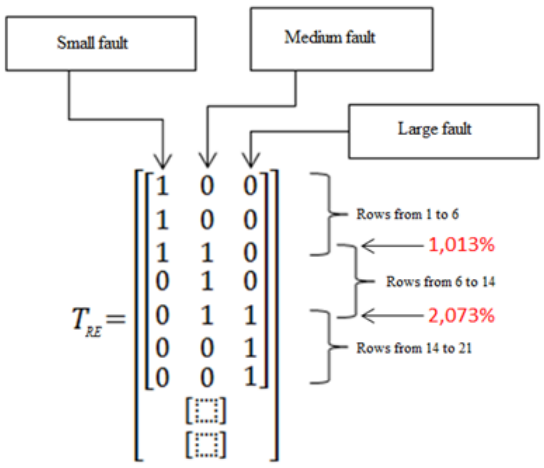

Figure 16. RE fault analysis - three columns target vector

References

[1]Çunkas, M., and Aydoğdu, O., "Realization of Fuzzy Logic Controlled Brushless DC Motor Drives using Matlab/Simulink", *Mathematical and Computational Applications*, Vol. 15, No. 02, pp. 218-229, 2010.

[2]Halvaei Niasar, A., Moghbelli, H., & Vahedi, A., "Modelling, Simulation and Implementation of Four-Switch Brushless DC Motor Drive Based On Switching Functions", *IEEE EUROCON 2009*, St.-Petersburg (Russia), 2009, pp. 682 – 687.

[3]Lee, B. K., Ehsani, M., "Advanced Simulation Model for Brushless DC Motor Drives", *Electric Power Components and Systems*, Vol. 31, No. 9, 2003, pp. 841–868, ISSN: 1532-5008.

[4]Hemanand, T., Rajesh, T., "Speed Control of Brushless DC Motor Drive Employing Hard Chopping PWM Technique Using DSP", *Proceedings of India International Conference on Power Electronics (IICPE 2006), 2006*.

[5]Haskew,T. A., Schinstock, D. E., & Waldrep E. M., "'Two-Phase On' Drive Operation in a Permanent Magnet Synchronous Machine Electromechanical Actuator", *IEEE Transactions on on Energy Conversion*, Vol. 14, No. 02, 1999.

[6]Borello, L., & Dalla Vedova, M. D. L., "A Dry Friction Model and Robust Computational Algorithm for Reversible or Irreversible Motion Transmission", *International Journal of Mechanics and Control (JoMaC)*, Vol. 13, No. 02, 2012, pp. 37-48.

[7]Borello, L., Dalla Vedova, M. D. L., Jacazio, G., and Sorli, M., "A Prognostic Model for Electrohydraulic Servovalves", *Proceedings of the Annual Conference of the Prognostics and Health Management Society*, San Diego (USA), 2009.

[8]Dalla Vedova, M. D. L., Jacazio, G., Maggiore, P., and Sorli, M., "Identification of Precursors of Servovalves Failures for Implementation of an Effective Prognostics", *International Conference of Recent Advances in Aerospace Actuation Systems and Components*. May 5-7, Toulouse (France), 2010, pp.116-126.

[9]Borello, L., Maggiore, P., Dalla Vedova, M. D. L., Alimhillaj, P., "Dry Fiction acting on Hydraulic Motors and Control Valves: Dynamic Behavior of Flight Controls", *XX National Congress AIDAA*. Milan (Italy), 2009.

[10]Borello, L., Maggiore, P., Villero, G., & Dalla Vedova, M. D. L., "A comparison between Dry Friction Discontinuous Computational Algorithms", *27th International Congress of the Aeronautical Sciences ICAS 2010*, Nice (France) ,2010.

[11]Borello, L., & Dalla Vedova, M. D. L., "Mechanical failures of flap control systems and related position errors: proposal of innovative configuration equipped with centrifugal brakes", *International Journal of Mechanics and Control (JoMaC)*, Vol. 07, No 02, 2006, pp. 7-20, ISSN: 1590-8844.

[12]Maggiore, P., Dalla Vedova, M. D. L., Pace, L., and Desando, A., "Definition of parametric methods for fault analysis applied to an electromechanical servomechanism affected by multiple failures," *Second European Conference of the Prognostics and Health Management Society*, Nantes (France), pp. 561-571, 2014.

[13]Welch, P. D., "The Use of Fast Fourier Transform for the Estimation of Power Spectra: A Method Based on Time Averaging Over Short, Modified Periodograms", *IEEE Transactions on audio and electroacoustics*, Vol. AU-15, No. 2, 1967.

[14]Cardona, A., Lerusse, A., & Géradin, M., "Fast Fourier nonlinear vibration analysis", *Computational Mechanics*, Vol. 22, No. 02, 1998, pp. 128-142.

[15]Chopra, I.,Ganguli, R.,Haas, D. J., "Detection of Helicopter Rotor System Simulated Faults Using Neural Networks", *Proceedings of the 37th Structures, Structural Dynamics and Materials Conference* (AIAA-96-1646-CP), Salt Lake City, Utah, 15-17 April 1996, pp. 1246-1263.

[16]Marquardt, D., "An Algorithm for Least-Squares Estimation of Nonlinear Parameters," *SIAM Journal on Applied Mathematics*, Vol. 11, No. 2, June 1963, pp. 431–441.

[17]Hagan, M.T., and M. Menhaj, "Training feed-forward networks with the Marquardt algorithm," *IEEE Transactions on Neural Networks*, Vol. 5, No. 6, 1999, pp. 989–993, 1994.